

Two Thieno[3,2-*b*]thiophene-Based Small Molecules as Bifunctional Photoactive Materials for Organic Solar Cells

Yunchuang Wang, Bin Kan, Xin Ke, Feng Liu, Xiangjian Wan,* Hongtao Zhang, Chenxi Li, and Yongsheng Chen*

Two bifunctional photovoltaic materials, named DRCN3TT and DRCN5TT with acceptor-donor-acceptor (A-D-A) type chemical structures based on thieno[3,2-*b*]thiophene central unit and 2-(1,1-dicyanomethylene)rhodanine terminal group, are designed and synthesized. Their thermal, optical and electrical properties are systematically investigated. The appropriate energy levels, both the electron and the hole transport properties and the appropriate molecular conformation make them work bifunctionally as both electron donor and acceptor for photovoltaic application. As donors, DRCN5TT and DRCN3TT based devices with [6,6]-phenyl-C₇₁-butyric acid methyl ester (PC₇₁BM) as acceptors show power conversion efficiencies (PCEs) of 7.03 and 3.85%, respectively. As acceptors, blended with the most profoundly studied donor materials such as poly(3-hexylthiophene) (P3HT) or its analogue PDCBT (poly[(4,4'-bis(2-butyloctoxycarbonyl)-[2,2'-bithiophene]-5,5'-diyl)-alt-(2,2'-bithiophene-5,5'-diyl)]), DRCN3TT and DRCN5TT show PCEs of 3–4%. The rarely studied bifunctional photovoltaic materials might provide another strategy to design new materials for high performance photovoltaic applications.

1. Introduction

Through decades of development, bulk heterojunction (BHJ) organic solar cells (OSCs) have become an established and increasingly important technology to meet the clean and renewable energy demand.^[1] Due to their advantageous properties of lightweight, low-cost, flexibility, and solution processability,^[2] tremendous work has been devoted to improving the device performance and the power conversion efficiencies (PCEs) of OSCs have already exceeded 13%.^[3] The state-of-the-art polymer- (P-OSCs)^[4] and small molecule- (SM-OSCs)^[5] based devices have made great strides with PCEs >11% based on fullerene derivatives,^[6] such as the classic [6,6]-phenyl-C₆₁-butyric acid methyl ester (PC₆₁BM) and [6,6]-phenyl-C₇₁-butyric acid methyl ester (PC₇₁BM), as acceptors. On the other hand, to overcome the shortcomings of fullerene-based acceptors,^[7] including poor light absorption, high-cost production and purification, restricted energy level tuning, and easy diffusion

and aggregation, new n-type materials are developed rapidly,^[8] and the PCE of fullerene-free solar cells have been elevated to over 13%,^[9] which has exceeded that of the fullerene-based solar cells. Thus, the design of both donors and acceptors is important for the development of OSCs.

A vast number of the photoactive materials reported so far exhibited unipolar photovoltaic properties, that is. they worked as either donor (p-type) or acceptor (n-type) materials. Unfortunately, bifunctional photovoltaic materials that combine both efficient donor and acceptor properties in the one molecule (namely one can function as donor material matched with such as PCBM or other acceptors and also serve as acceptor when combined with donor such as P3HT) rarely appear in literatures.^[10] Bifunctional photovoltaic material is favorable not only for the understanding of chemical structure-properties-device performance relationships but also for easier and more efficient material design and preparation. It is important to note that many issues, such as appropriate energy levels, ambipolar charge transport properties, and appropriate self-aggregation, are all important for realizing the dual functionality in

Y. Wang, B. Kan, X. Ke, Dr. X. Wan, Dr. H. Zhang, Prof. C. Li, Prof. Y. Chen
The Centre of Nanoscale Science and Technology and Key Laboratory of Functional Polymer Materials
State Key Laboratory and Institute of Elemento-Organic Chemistry
College of Chemistry
Nankai University
Tianjin 300071, China
E-mail: xjwan@nankai.edu.cn; yschen99@nankai.edu.cn

Y. Wang, B. Kan, X. Ke, Dr. X. Wan, Dr. H. Zhang, Prof. C. Li, Prof. Y. Chen

The National Institute for Advanced Materials
Nankai University
Tianjin 300071, China

Dr. F. Liu
Department of Physics and Astronomy
Shanghai Jiaotong University
Shanghai 200240, China

 The ORCID identification number(s) for the author(s) of this article can be found under <https://doi.org/10.1002/solr.201700179>.

DOI: 10.1002/solr.201700179

photovoltaic devices. With the advantages of well-defined chemical structures and less batch-to-batch variations, easier energy level control and etc.,^[6b,11] small molecules are believed to be the candidates for high performance bifunctional photovoltaic materials.

Recently, our group has reported a series of oligomer-like small molecule donor materials DRCN4T-DRCN9T with 4 to 9 thiophene units in the backbones. Among them, DRCN5T exhibited an outstanding PCE >10%.^[5b] This work and many other reports^[5b,12] have demonstrated that the conjugation length has significant impact on the molecular orbital energy levels, molecular packing and charge carrier mobility. The thieno[3,2-*b*]thiophene (TT) unit is of particular interest in the design of low band gap conjugated polymers for high-performance organic field-effect transistors and OSCs due to its stable quinoidal structure.^[13] DRCN8TT, using TT as the core blocking unit to replace the central thiophene of DRCN7T, possesses nonplanar backbone conformation and still performs a high PCE of 8.11% in our previous work.^[14] It was found that the introduction of TT unit could break the coplanarity of the conjugated backbone of the DRCN7T molecule. On the other hand, it has been widely known that the highest occupied molecular orbital (HOMO) will go down with decreasing the conjugation length of the conjugated molecules. Therefore, we propose that the introduction of TT unit into the DRCN5T and DRCN3T might give molecules suitable energy levels as bifunctional materials. The dihedral angles between TT unit and their adjacent thiophene units for DRCN3TT and DRCN5TT calculated by the density functional theory are 16.4° and 25.1°, respectively. Thus the non-coplanarity of the two molecules might ensure an appropriate phase separation when they are used as acceptors in the OSC devices. The above properties make DRCN3/5TT qualify as bifunctional materials, that is both electron donors and acceptors in the OSC devices.

Taking account of the above considerations, we herein have designed and synthesized two small molecules DRCN3TT and DRCN5TT with TT as the central unit (Figure 1). Systematic

characterizations indicated that the two molecules both exhibited bifunctional properties, i.e. they can be used as both donors and acceptors for photovoltaic devices. As donors and blending with conventional acceptor PC₇₁BM, DRCN5TT, and DRCN3TT based devices gave PCEs of 7.03 and 3.85%, respectively. When used as acceptors in P3HT-based devices, DRCN3TT and DRCN5TT gave PCEs of 3.55 and 2.78%, respectively, and a higher PCE of 4.08% device can be achieved by combing PDCBT donor material with DRCN3TT acceptor. The nonplanar backbone resulted from the introduction of TT building block is crucially important for the bifunctional properties of the two small molecules. These results could give valuable insight on the molecular design and the study about the correlations between molecular chemical structures and properties.

2. Results and Discussion

2.1. Synthesis and Thermal Property

The synthetic routes for DRCN3TT and DRCN5TT are presented in Scheme S1 (Supporting Information) and the detailed procedures were described in the Supporting Information. The important intermediates DF3TT and DF5TT (Scheme S1) were synthesized using Pd(PPh₃)₄-catalyzed Stille coupling from the 2,5-dibromothiopheno[3,2-*b*]thiophene. The targeted molecules were then prepared by Knoevenagel condensation of DF3/5TT with 2-(3-ethyl-4-oxothiazolidin-2-ylidene)-malononitrile. Thermogravimetric analysis (TGA) indicates the two molecules both possess good thermal stability with a 5% weight loss (*T_d*) occurring over 380 °C under nitrogen atmosphere (Figure S1a, Supporting Information). Differential scanning calorimetry (DSC) analysis (Figure S1b, Supporting Information) shows that clear melting temperatures (*T_m*) upon the heating process and recrystallization points (*T_{cr}*) upon the cooling process are observed for the two molecules, which means that DRCN3/5TT both possess good crystallization properties.^[15]

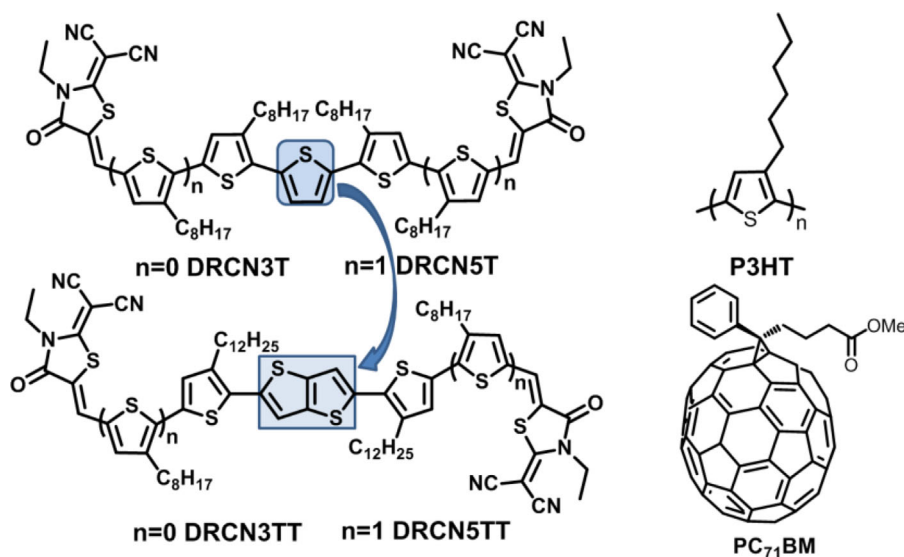


Figure 1. Chemical structures of DRCN3T, DRCN5T, DRCN3TT, DRCN5TT, P3HT, and PC₇₁BM.

2.2. Optical Absorption and Electrochemical Properties

The ultraviolet-visible (UV-vis) absorption spectra of these two molecules in diluted chloroform (CHCl_3) and in the solid state are shown in **Figure 2** and the corresponding data are listed in **Table 1**. In solution, DRCN3TT and DRCN5TT showed two distinct absorption bands in the shorter wavelength region (300–450 nm) and in the longer wavelength region (450–600 nm), with maxima extinction coefficients (ϵ) of 6.4×10^4 and $7.5 \times 10^4 \text{ M}^{-1} \text{ cm}^{-1}$, respectively. As shown in **Figure 2b**, the normalized thin-film absorption spectra of two molecules display an obvious red-shifted (59 nm for DRCN3TT and 72 nm for DRCN5TT, respectively) and a broadened absorption range compared with that of their solution absorption. In DRCN3TT neat film, a new absorption peak at ≈ 640 nm appeared, indicating that intermolecular π - π interactions were obvious in the solid state. The absorption peak of DRCN5TT is red-shifted by 13 nm compared to DRCN3TT, which may be attributed to the longer conjugation length of DRCN5TT. For the as-cast films, the absorption onsets of DRCN3TT is at ca. 720 nm, while that of DRCN5TT is ca. 760 nm, corresponding to the optical band gap of 1.72 and 1.63 eV, respectively.

Cyclic voltammetry (CV) measurement was performed to investigate the molecules' energy levels. As depicted in **Figure S2a** (Supporting Information), the HOMO and the lowest unoccupied molecular orbital (LUMO) levels are -5.44 and -3.50 eV for DRCN3TT, and -5.22 and -3.52 eV for DRCN5TT respectively, calculated from the onset oxidation and reduction potential. Density functional theory (DFT) calculation at the B3LYP/6-31G level was also employed to investigate the optimized geometry (**Figure S4**, Supporting Information) and electronic structure (**Figure S5**, Supporting Information) of the two molecules. The optimized geometries for DRCN3/5TT are centro-symmetric structures. It is worthy to note that the molecular backbones of DRCN3/5TT are not planar, showing dihedral angles of 16.4° and 25.1° between the TT unit and its adjacent thiophene unit. DRCN3/5TT are expected to exhibit weak self-aggregation because of their nonplanar structures, which might ensure an appropriate phase separation and exciton dissociation efficiency for the non-fullerene OSCs.^[11a]

2.3. Bifunctional Properties

The appropriate HOMO/LUMO energy levels of DRCN3/5TT together with their narrow band gaps and twisted molecular conformations may enable them to behave as ambipolar semiconductors.^[16] As illustrated in **Figure 2c**, both HOMO and LUMO energy levels of DRCN3/5TT are lower than those of P3HT (4.93 and 2.55 eV) (**Figure S2b**, Supporting Information), but higher than those of PC₇₁BM (5.87 and 3.91 eV).^[17] The offsets of LUMOs between DRCN3/5TT and P3HT or PC₇₁BM are large enough to ensure the charge separation. The photoluminescence (PL) spectra (**Figure S6**, Supporting Information) show that blending DRCN3/5TT with PC₇₁BM or P3HT led to significant fluorescence quenching, indicating that effective photoinduced charge transfer occurred between DRCN3/5TT and PC₇₁BM or P3HT in the blend films. The charge-transport properties of DRCN3/5TT were investigated using the space charge limited current (SCLC) method.^[18] The $J^{0.5}$ - V characteristics of the hole-only and electron-only devices based on the as-cast DRCN3/5TT films are provided in **Figure S7** (Supporting Information). From **Figure S7**, the electron and hole mobilities are 1.48×10^{-4} and $8.18 \times 10^{-5} \text{ cm}^2 \text{ V}^{-1} \text{ s}^{-1}$ for DRCN3TT and 7.05×10^{-5} and $9.01 \times 10^{-5} \text{ cm}^2 \text{ V}^{-1} \text{ s}^{-1}$ for DRCN5TT, respectively. The somehow balanced bipolar charge-transport property and the above findings about their HOMO/LUMO levels of DRCN3/5TT make them qualified as bifunctional materials, that is both electron donors and acceptors in the OSC devices.

2.4. Photovoltaic Properties and Characterization

2.4.1. As Electron Donor for Photovoltaic Devices

Solution-processed BHJ devices with a conventional structure of ITO/PEDOT:PSS/active layer/PFN-Br/Al and PC₇₁BM as the acceptor were firstly fabricated to evaluate the performance of DRCN3/5TT as electron donors. The current density-voltage (J - V) and external quantum efficiency (EQE) curves for the optimized devices are shown in **Figure 3a-b** and the corresponding photovoltaic parameters are summarized in **Table 2**. The devices of DRCN5TT:PC₇₁BM gave a PCE of 7.03%, with an

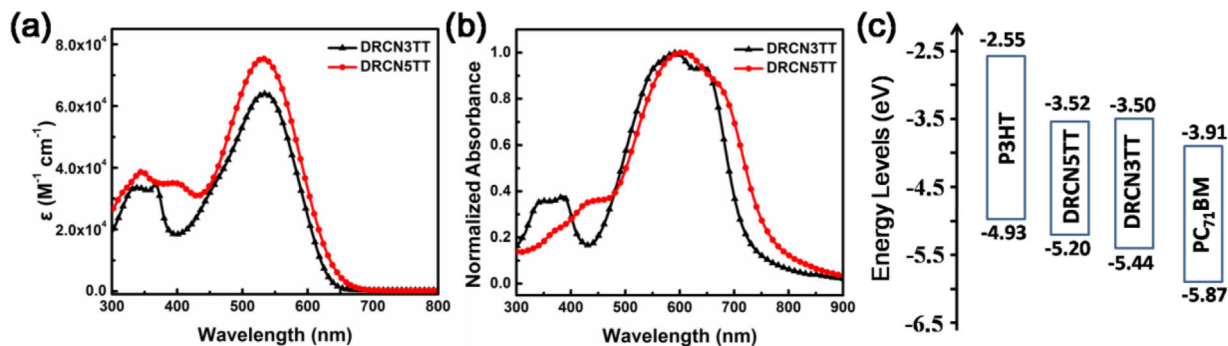


Figure 2. a) UV-vis absorption spectra of DRCN3/5TT in chloroform solution; b) Normalized UV-vis absorption spectra of DRCN3TT and DRCN5TT in the film state; c) Schematic energy-level diagrams of P3HT, DRCN3TT, DRCN5TT, and PC₇₁BM.

Table 1. Optical and electrochemical data of DRCN3/5TT.

Molecules	Film absorption			CV		Mobility	
	λ_{\max} (nm)	λ_{onset} (nm)	E_g^{opt} (eV)	HOMO (eV)	LUMO (eV)	μ_h ($\text{cm}^2\text{V}^{-1}\text{s}^{-1}$)	μ_e ($\text{cm}^2\text{V}^{-1}\text{s}^{-1}$)
DRCN5TT	605, 642	770	1.63	-5.22	-3.52	9.01×10^{-5}	7.05×10^{-5}
DRCN3TT	592	720	1.72	-5.44	-3.50	8.18×10^{-5}	1.48×10^{-4}
P3HT	528	646	1.92	-4.93	-2.55	-	-
PC ₇₁ BM ^{a)}	-	709	1.75	-5.87	-3.91	-	-

^{a)}The data from Ref. [17].

open-circuit voltage (V_{oc}) of 0.90 V, a fill factor (FF) of 0.629, and a short-circuit current density (J_{sc}) of 12.43 mA cm^{-2} . In contrast, a lower PCE of 3.85% was obtained for DRCN3TT based devices. As expected, with the decrease of the conjugation length, DRCN3TT showed higher V_{oc} of 0.94V than that of DRCN5TT, also consistent with the trend of their HOMO levels. DRCN3TT showed relatively weak UV-vis absorption due to its short backbone conjugation length in contrast to that of DRCN5TT (Figure S16a), which is one of the factors that give low J_{sc} of

DRCN3TT based devices. As shown in Figure 3b, external quantum efficiency (EQE) of DRCN5TT based device exhibits photo-current responses from 300 to 800 nm with a maximum value of 61%. In contrast, the onset photovoltaic responses of DRCN3TT based device ends at ca. 720 nm and the value is far smaller than that of DRCN5TT across the whole wavelength range. By integrating the EQE spectra, the calculated J_{sc} of 6.04 and 12.06 mA cm^{-2} were obtained for DRCN3TT and DRCN5TT based devices, respectively, which were in good agreement with J - V measurements.

The curves of photogenerated current density (J_{ph}) versus effective voltage (V_{eff}) were also measured (Figure S17).^[19] The charge dissociation and charge collection probability ($P(E, T)$) in the devices could be estimated by calculating the value of $J_{\text{ph}}/J_{\text{sat}}$, where J_{sat} stands for saturation photocurrent density. Under the short-circuit and maximal power output conditions, $P(E, T)$ values are 90%, 70% for the DRCN5TT:PC₇₁BM based device, and 83%, 65% for the device based on DRCN3TT:PC₇₁BM. The higher $P(E, T)$ values indicate that DRCN5TT:PC₇₁BM based device exhibits higher exciton dissociation and more efficient charge collection efficiency compared to those of DRCN3TT:PC₇₁BM based device.

The optimized morphologies of the active layers were measured by atomic force microscopy (AFM) and transmission electron microscopy (TEM). As depicted in Figure S18b (Supporting Information), it can be seen that the surface of DRCN5TT:PC₇₁BM blend film is uniform and smooth with root-mean-square (rms) surface roughness values of 0.89 nm with well-interpenetrating networks indicative of obvious phase separation. DRCN3TT can also form smooth surfaces with rms of 1.31 nm when it is blended with PC₇₁BM, as shown in Figure S16a. From the TEM images (Figure 4a and b), DRCN5TT:PC₇₁BM blend film showed a better ordered fibrillar structure and smaller domain sizes in comparison to DRCN3TT:PC₇₁BM film. Resonant soft X-ray scattering (RSoXS) (Figure S19, Supporting Information) on the small

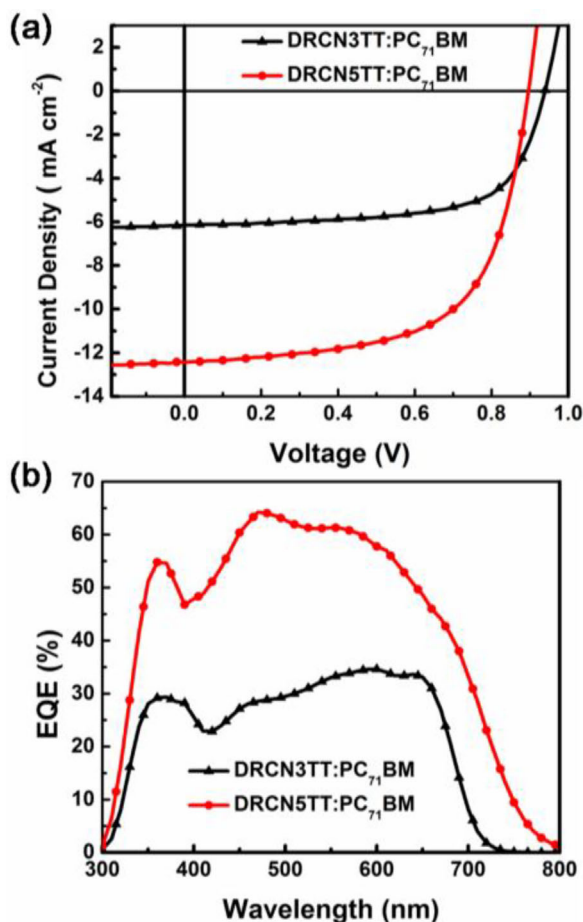


Figure 3. a) Current density versus voltage (J - V) curves; b) External quantum efficiency (EQE) spectra of the best-performing DRCN5TT and DRCN3TT-based fullerene OSCs.

Table 2. The optimized photovoltaic parameters of devices based on DRCN3/5TT and PC₇₁BM.

Materials	V_{oc} [V]	$J_{\text{sc}}^{\text{a)}$ [mA cm^{-2}]	FF [%]	PCE ^{b)} [%]
DRCN3TT:PC ₇₁ BM	0.94	6.15 (6.04)	66.6	3.85 (3.64)
DRCN5TT:PC ₇₁ BM	0.90	12.43 (12.06)	62.9	7.03 (6.71)

^{a)}The J_{sc} in brackets was obtained by integrating the EQE of devices; ^{b)}The average PCEs in brackets were obtained from 15 devices.

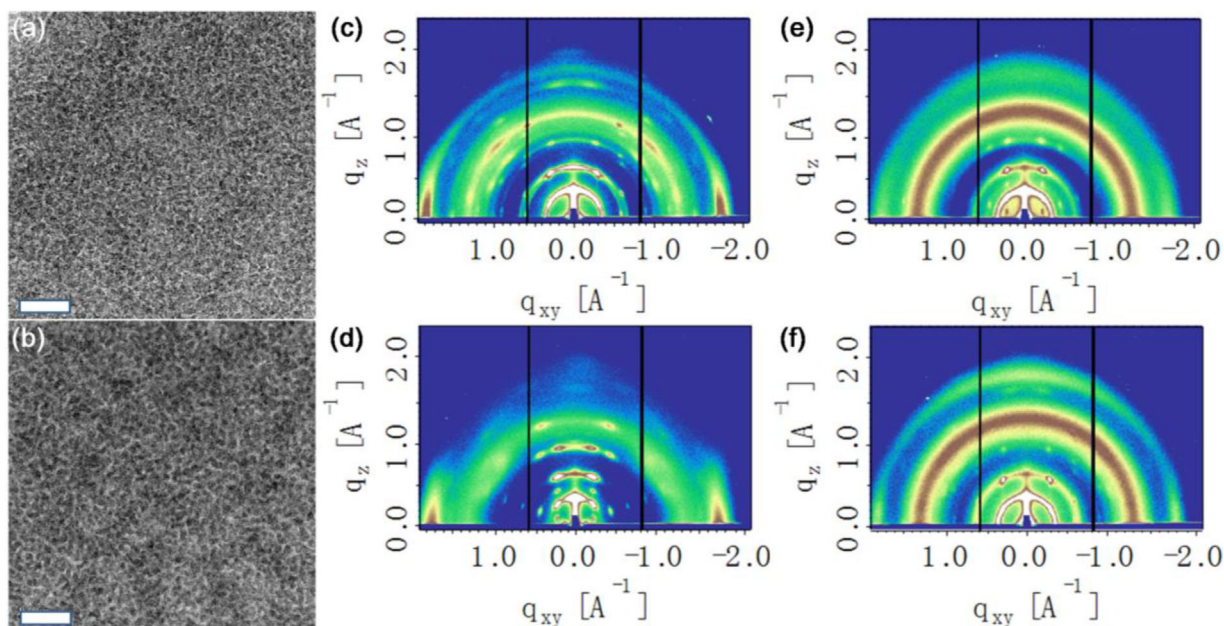


Figure 4. TEM images of the active layers: a) DRCN3TT:PC71BM, b) DRCN5TT:PC71BM, under their optimized conditions; GIXD for pure films of c) DRCN3TT, d) DRCN5TT and blend films of e) DRCN3TT:PC71BM, f) DRCN5TT:PC71BM. The scale bars are 200 nm.

molecule:PC₇₁BM blend film shows an interference ($q = 0.012$ and 0.014 \AA^{-1}) corresponding to a domain center-to-center distance of 52 and 45 nm for DRCN3TT and DRCN5TT, respectively. The RSoXS results show similar tendency with the morphologies observed by TEM, supporting the higher J_{sc} of DRCN5TT-based solar cells.

The microstructures of DRCN3/5TT films and their optimized blend films were characterized by two-dimensional grazing incidence X-ray diffraction (2D-GIXD). Out-of-plane and in-plane line cuts of GIXD of blend films are presented in Figure S20 (Supporting Information). As can be seen from Figure 4c and d, DRCN3TT and DRCN5TT both exhibit obvious (010) diffraction peaks in the in-plane direction and (100) diffraction peaks in the out-of-plane direction, suggesting that DRCN3TT and DRCN5TT both have an edge-on orientation relative to the substrate. When these molecules served as donor materials blended with PC₇₁BM, multiple higher order (h00) reflections along the q_z direction are observed for both molecules, indicative of a long-range order and crystallinity in the blend films of both molecules. The (100) peaks along the q_z direction of DRCN3/5TT are both observed at 0.34 and 0.33 \AA^{-1} , corresponding to their alkyl-to-alkyl distance of 18.5 and 19.0 Å, respectively. The (010) π - π stacking peaks appeared in both q_{xy} and q_z directions for both molecules, indicating mixed edge-on and face-on orientations. The more obvious (010) peak and shorter π - π stacking distance of DRCN3TT-based active layer suggested its more ordered structure than that of DRCN5TT-based film, which is beneficial for charge transport and thus higher FF of DRCN3TT-based devices.^[20] Combination with their fully planar analogue DRCN5T, which shows a prominent face-on orientation when blended with PC₇₁BM,^[5b] it can be seen that the less ordered structures might result from the nonplanar backbone

of the molecules, which is unfavorable for charge transport, thus leading to a low FF.

2.4.2. As Electron Acceptor for Photovoltaic Devices

Next, these two molecules used as the electron acceptor with the widely used conventional donor material P3HT were investigated with the BHJ devices configuration of ITO/PEDOT:PSS/active layer/ZnO nanoparticles/Al. The J - V curves and EQE spectra of the two molecules based optimized devices are shown in Figure 5a and b and the relevant photovoltaic parameters are listed in Table 3. After thermal annealing (TA), P3HT:DRCN3TT based device achieved a PCE of 3.55%, with V_{oc} of 0.90 V, FF of 0.501, and a J_{sc} of 7.87 mA cm^{-2} . However, the device of P3HT:DRCN5TT gave a lower PCE of 2.78%, with V_{oc} of 0.92 V, FF of 0.503, and a J_{sc} of 6.02 mA cm^{-2} . Note the devices with these two molecules as the electron acceptor behaved quite normal particularly in the terms of the V_{oc} . The lower FF and J_{sc} are the deteriorating factors that brings down the device performance, which will be discussed later. From Figure S16b (Supporting Information), it can be clearly seen that the absorption intensity of P3HT:DRCN3TT film is higher than that of the P3HT:DRCN5TT film, which favors the higher J_{sc} of P3HT:DRCN3TT based devices. As shown in the EQE curves (Figure 5b), P3HT:DRCN3TT based devices show a much higher EQE values than that of P3HT:DRCN5TT devices in the whole absorption range from 300 to 700 nm. The calculated J_{sc} by integration of the EQE curves are 5.73 and 7.64 mA cm^{-2} for P3HT:DRCN5TT and P3HT:DRCN3TT based devices, respectively. The narrow spectral response, only across the wavelength range of 300-700 of these two molecules based nonfullerene OSCs resulted from

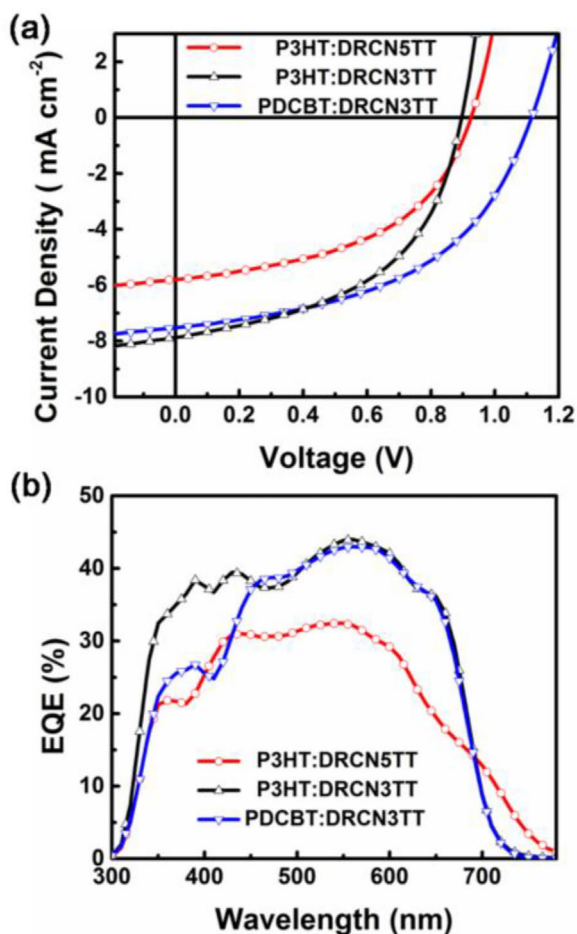


Figure 5. a) J - V curves; b) EQE spectra of DRCN3/5TT based non-fullerene OSCs.

the absorption of the blend films, is unfavorable for the improvement of J_{sc} .

AFM and TEM were also performed to investigate the morphology of the active layer. As shown in the AFM images (Figure S18, Supporting Information), the P3HT:DRCN5TT blend film can form smooth surface with an rms of 1.59 nm and the P3HT:DRCN5TT film gets a smaller rms of 0.91 nm. As seen from the TEM images (Figure 6a and b) and the RSoXS measurement (Figure 6c), P3HT:DRCN5TT film showed an unapparent phase separation of donor and acceptor and scattering signal across a

Table 3. Photovoltaic performance parameters of DRCN3/5TT based non-fullerene OSCs.

Materials	V_{oc} [V]	J_{sc}^a [mA cm^{-2}]	FF [%]	PCE ^b [%]
P3HT:DRCN5TT	0.92	6.02 (5.73)	50.3	2.78 (2.68)
P3HT:DRCN3TT	0.90	7.87 (7.64)	50.1	3.55 (3.35)
PDCBT:DRCN3TT	1.11	7.52 (7.26)	48.9	4.08 (3.81)

^aThe J_{sc} in brackets was obtained by integrating the EQE of devices; ^bThe average PCEs in brackets were obtained from 15 devices.

broad q region from 0.003 – 0.01 \AA^{-1} , while P3HT:DRCN5TT based film showed no scattering signal. The RSoXS results showed similar tendency as that of the TEM and AFM images, indicating enhanced phase separation of P3HT:DRCN3TT film, agree with the higher J_{sc} of P3HT:DRCN5TT based device. However, the phase separation of P3HT:DRCN3TT is insufficient for efficient exciton dissociation/separation and charge transport, and thus comparatively lower J_{sc} and FF.

When the two small molecules were blended with P3HT, strong π - π stacking diffractions in the out-of-plane direction were observed in the two blend films. For the P3HT:DRCN3TT blends, the DRCN3TT crystalline structure was preserved which can be deduced from the broad and diffuse isotropic peak at $\approx 1.3 \text{ \AA}^{-1}$. The P3HT (100) peak at 0.35 \AA^{-1} with a distance of 17.9 Å is coincident with alkyl-alkyl spacing of DRCN3TT. The crystal size from Scherrer analysis was 81 Å. The (010) π - π stacking peaks appeared in the out-of-plane direction at 1.74 \AA^{-1} , corresponding to a π - π stacking distance of 3.61 Å with crystal size of 34.2 Å. In the P3HT:DRCN5TT blend film, the acceptor also shows good crystalline order and the (100) peak in the out-of-plane direction was decomposed into two distinct reflections at 0.36 and 0.26 \AA^{-1} . The 0.36 \AA^{-1} peak, corresponding to an alkyl-to-alkyl distance of 17.4 Å, arises from the (100) reflection of P3HT (110 Å in crystal size) and the 0.26 \AA^{-1} peak, corresponding to the distance of 24.2 Å, arises from the (100) reflection of DRCN5TT (144 Å in crystal size). A 3.80 Å π - π stacking distance is seen and a crystal with size of 52.9 Å is formed in the out-of-plane profiles, which are much larger than those of P3HT:DRCN3TT and unfavorable for charge transport.

In addition, we also combined the analogue of P3HT, namely, PDCBT (poly[(4,4'-bis(2-butyloctoxycarbonyl)-[2,2'-bithiophene]-5,5-diyl)-alt-(2,2'-bithiophene-5,5'-diyl)]) consisting of alkoxy carbonyl-functionalized polythiophene (Figure S21, Supporting Information), with DRCN3TT to fabricate the nonfullerene OSCs. In comparison with the OSCs based on P3HT:DRCN3TT, the PDCBT:DRCN3TT based non-fullerene devices showed improved PCE of 4.08% with similar J_{sc} (7.52 mA cm^{-2}) and FF (0.489) but higher V_{oc} of 1.11 V (Figure 5), originating from the deeper HOMO level of PDCBT.^[21]

As discussed above, DRCN5TT based fullerene OSC performs better than that of DRCN3TT based devices, resulted from the much higher J_{sc} . The low FF of DRCN5TT:PC₇₁BM based device is consistent with the mixed edge-on and face-on orientations of DRCN5TT in the blend film. When applied in P3HT-based nonfullerene OSCs, DRCN3TT which contains shorter conjugated length give a little higher PCE than that of DRCN5TT. In comparison with the high performance non-fullerene OSCs in literatures, the much lower J_{sc} and FF should be responsible for the low photovoltaic performance. The absorption spectra of these two molecules ending at the wavelength of $\approx 700 \text{ nm}$ significantly restrict the J_{sc} of these two molecules based nonfullerene devices. And the nonplanar structures of these two molecules derived from the conjugated backbone are not sufficient for providing appropriate phase separation with the polymer donors and thus lower FF. It is believable that a high nonfullerene OSCs can be achieved through the optimization of the molecular structure and morphology control.

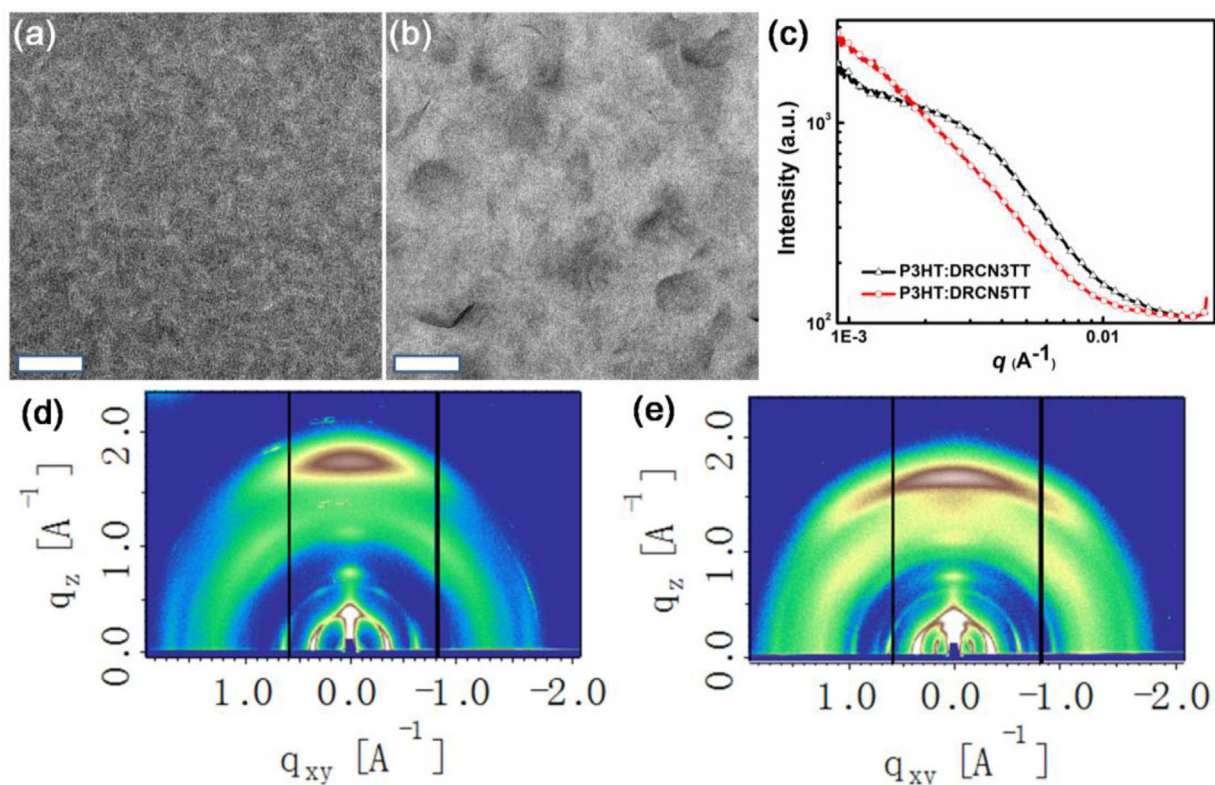


Figure 6. TEM images of the active layers: a) P3HT:DRCN3TT and b) P3HT:DRCN5TT; c) RSoXS profiles of P3HT:DRCN3TT and P3HT:DRCN5TT; GIXD for d) P3HT:DRCN3TT, e) P3HT:DRCN5TT with TA treatment. The scale bars are 200 nm.

3. Conclusion

In summary, two bifunctional photovoltaic A-D-A small molecule materials, namely DRCN3TT and DRCN5TT, containing the same electron-rich TT subunit as core building block and end-capped with 2-(1,1-dicyanomethylene)rhodanine, were designed and synthesized. The two small molecules show high ambipolar charge mobility and could be used as donors or acceptors in the organic solar cells, rarely studied so far. When they worked as donors with PC₇₁BM, DRCN5TT and DRCN3TT gave PCEs of 7.03 and 3.85%, respectively. Their performance as the electron acceptor with P3HT as the donor. But a PCE of 4.08% was achieved for the devices using DRCN3TT as the acceptor and polymer PDCBT as donor with a high V_{oc} of 1.11V. The different performance of these two molecules when used as donor and acceptor materials are believed mainly due to the corresponding morphology difference as the devices all behavior normally with appropriate V_{oc} but low FF and J_{sc} in the case as electron acceptor. Thus, although the PCEs for these solar cells are currently low, it is believed that the performance can be enhanced by further optimization of molecular structure and morphology control. Through comparisons of the photovoltaic performance of DRCN3TT and DRCN5TT based different type devices, we demonstrated that there is a complicated balance between the molecular conjugation length and the roles they served in different type devices blended with donor

or acceptor materials. These results could give some valuable insight for designing new bifunctional photovoltaic molecules for the high efficient OSCs.

4. Experimental Section

General Experimental Details: All reactions and manipulations were carried out in a argon atmosphere atmosphere with the use of standard Schlenk techniques. 2-bromo-3-dodecylthiophene (3), 5-bromo-4-octylthiophene-2-carbaldehyde (Compound 6), 5'-bromo-3,4'-dioctyl-[2,2'-bithiophene]-5-carbaldehyde (Compound 7) were prepared according to literature procedures.^[22] Other starting materials were purchased from commercial suppliers and used as received unless indicated otherwise. The ¹H and ¹³C NMR spectra were recorded on a Bruker AV400 Spectrometer. Matrix assisted laser desorption/ionization time-of-flight mass spectrometry (MALDI-TOF) were performed on a Bruker Autoflex III LRF200-CID instrument. The thermogravimetric analysis (TGA) was carried out on a NETZSCH STA 409PC instrument under purified nitrogen gas flow with a 10 °C min⁻¹ heating rate. UV-Vis spectra were obtained with a JASCO V-570 spectrophotometer.

Cyclic voltammetry (CV) experiments were performed with a LK98B II Microcomputer-based Electrochemical Analyzer. All CV measurements were carried out at room temperature with a conventional three-electrode configuration employing a glassy carbon electrode as the working electrode, a saturated calomel electrode (SCE) as the reference electrode, and a Pt wire as the counter electrode. Dichloromethane was distilled from calcium hydride under dry nitrogen immediately prior to use. Tetrabutylammonium phosphorus hexafluoride (Bu₄NPF₆, 0.1M) in dichloromethane was used as the supporting electrolyte, and the scan

rate was 100 mVs^{-1} . The highest occupied molecular orbital (HOMO) and lowest unoccupied molecular orbital (LUMO) energy levels were calculated from the onset oxidation potential and the onset reduction potential, using the equation $E_{\text{HOMO}} = -(4.80 + E_{\text{onset}}^{\text{ox}})$, $E_{\text{LUMO}} = -(4.80 + E_{\text{onset}}^{\text{re}})$.

The geometry structures of DRCN3TT and DRCN5TT were optimized by using DFT calculations (B3LYP/6-31G*), and the frequency analysis was followed to ensure that the optimized structures were stable states. All calculations were carried out using Gaussian 09.

Atomic force microscopy (AFM) was performed using Multimode 8 atomic force microscope in tapping mode. The transmission electron microscopy (TEM) investigation was performed on Philips Technical G2 F20 at 200 kV. The specimen for TEM measurement was prepared by spin casting the blend solution on ITO/PEDOT:PSS substrate, then floating the film on a water surface, and transferring to TEM grids. Grazing incidence wide-angle X-ray scattering (GIXD) and resonant soft X-ray scattering (RSOXS) were performed at beam line 7.3.3 and 11.0.1.2 at Lawrence Berkeley National Lab.

Space charge limited current (SCLC) mobility was measured using a diode configuration of ITO/PEDOT:PSS/small molecule/Au for hole mobility and glass/Al/small molecule/Al for electron mobility and fitting the results to a space charge limited form, where the SCLC equation is described by

$$J = \frac{9\epsilon_0\epsilon_r\mu_0V^2}{8L^3}$$

where J is the current density, L is the film thickness of the active layer, μ_0 is the hole or electron mobility, ϵ_r is the relative dielectric constant of the transport medium, ϵ_0 is the permittivity of free space ($8.85 \times 10^{-12}\text{ F m}^{-1}$), V ($=V_{\text{appl}} - V_{\text{bi}}$) is the internal voltage in the device, where V_{appl} is the applied voltage to the device and V_{bi} is the built-in voltage due to the relative work function difference of the two electrodes.

Solar Cell Fabrication and Testing: The devices were fabricated with a structure of glass/ITO/PEDOT:PSS/donor:acceptor/ETL/Al. The ITO-coated glass substrates were cleaned by ultrasonic treatment in detergent, deionized water, acetone, and isopropyl alcohol under ultrasonication for 15 minutes each and subsequently dried by a nitrogen blow. A thin layer of PEDOT:PSS (Clevios P VP Al 4083, filtered at $0.45\ \mu\text{m}$) was spin-coated at 4000 rpm onto ITO surface. After baked at 150°C for 20 min, the substrates were transferred into an argon-filled glove box. Subsequently, the active layer was spin-coated from blend chloroform solutions of donor and acceptor. Then, for the fullerene-based solar cells, the substrates were placed in a glass petri dish containing 1 ml tetrahydrofuran for 1 minute for solvent vapor annealing (SVA) and PFN-Br solution (0.5 mg mL^{-1} , dissolved in methanol) was spin-coated at 3000 rpm; with regard to the fullerene free solar cells, the substrates were annealed at 140°C for 10 min and the ZnO nanoparticles were spin-coated at 3000 rpm. Finally, 80 nm Al layer were deposited under high vacuum ($<2 \times 10^{-4}\text{ Pa}$). The current density-voltage (J - V) curves of photovoltaic devices were obtained by a Keithley 2400 source-measure unit. The photocurrent was measured under illumination simulated 100 mW cm^{-2} AM 1.5G irradiation using an Oriel 96000 solar simulator, calibrated with a standard Si solar cell. The average PCE was obtained using 15 devices under the same conditions. External quantum efficiencies were measured using Stanford Research Systems SR810 lock-in amplifier. The thickness of the active layers in the photovoltaic devices was measured on a Veeco Dektak 150 profilometer.

Supporting Information

Supporting Information is available from the Wiley Online Library or from the author.

Acknowledgements

The authors gratefully acknowledge the financial support from MoST (No. 2014CB643502) and NSFC (Nos. 91433101, 91633301) of China and Tianjin city (17JCZDJC31100).

Conflict of Interest

The authors declare no conflict of interest.

Keywords

bifunctional photoactive materials, small-molecule solar cells, thieno[3,2-*b*]thiophene

Received: October 24, 2017

Revised: November 18, 2017

Published online:

- [1] a) S. Günes, H. Neugebauer, N. S. Sariciftci, *Chem. Rev.* **2007**, *107*, 1324; b) R. F. Service, *Science* **2011**, *332*, 293; c) G. Li, R. Zhu, Y. Yang, *Nat. Photonics* **2012**, *6*, 153; d) C. J. Brabec, N. S. Sariciftci, J. C. Hummelen, *Adv. Funct. Mater.* **2001**, *11*, 15; e) T. Ameri, P. Khoram, J. Min, C. J. Brabec, *Adv. Mater.* **2013**, *25*, 4245.
- [2] a) G. Yu, J. Gao, J. C. Hummelen, F. Wudl, A. J. Heeger, *Science* **1995**, *270*, 1789; b) F. C. Krebs, *Sol. Energy Mater. Sol. Cells* **2009**, *93*, 394.
- [3] a) M. Li, K. Gao, X. J. Wan, Q. Zhang, B. Kan, R. Xia, F. Liu, X. Yang, H. Feng, W. Ni, Y. Wang, J. Peng, H. Zhang, Z. Liang, H.-L. Yip, X. Peng, Y. Cao, Y. Chen, *Nat. Photonics* **2017**, *11*, 85; b) W. Zhao, S. Li, H. Yao, S. Zhang, Y. Zhang, B. Yang, J. Hou, *J. Am. Chem. Soc.* **2017**, *139*, 7148; c) Y. Cui, H. Yao, B. Gao, Y. Qin, S. Zhang, B. Yang, C. He, B. Xu, J. Hou, *J. Am. Chem. Soc.* **2017**, *139*, 7302.
- [4] a) S. H. Liao, H. J. Jhuo, P. N. Yeh, Y. S. Cheng, Y. L. Li, Y. H. Lee, S. Sharma, S. A. Chen, *Sci. Rep.* **2014**, *4*, 6813; b) J. Huang, C. Z. Li, C. C. Chueh, S. Q. Liu, J. S. Yu, A. K. Y. Jen, *Adv. Energy Mater.* **2015**, *5*, 1500406; c) X. Ouyang, R. Peng, L. Ai, X. Zhang, Z. Ge, *Nat. Photonics* **2015**, *9*, 520; d) J. Zhao, Y. Li, G. Yang, K. Jiang, H. Lin, H. Ade, W. Ma, H. Yan, *Nat. Energy* **2016**, *1*, 15027; e) J. D. Chen, C. Cui, Y. Q. Li, L. Zhou, Q. D. Ou, C. Li, Y. Li, J. X. Tang, *Adv. Mater.* **2015**, *27*, 1035; f) X. Liu, X. Li, Y. Li, C. Song, L. Zhu, W. Zhang, H. Wang, J. Fang, *Adv. Mater.* **2016**, *28*, 7405; g) Q. Wan, X. Guo, Z. Wang, W. Li, B. Guo, W. Ma, M. Zhang, Y. Li, *Adv. Funct. Mater.* **2016**, *26*, 6635; h) J. Huang, X. Zhang, D. Zheng, K. Yan, C.-Z. Li, J. Yu, *Sol. RRL* **2017**, *1*, 1600008.
- [5] a) Y. Liu, C. C. Chen, Z. Hong, J. Gao, Y. M. Yang, H. Zhou, L. Dou, G. Li, Y. Yang, *Sci. Rep.* **2013**, *3*, 3356; b) B. Kan, M. Li, Q. Zhang, F. Liu, X. Wan, Y. Wang, W. Ni, G. Long, X. Yang, H. Feng, Y. Zuo, M. Zhang, F. Huang, Y. Cao, T. P. Russell, Y. Chen, *J. Am. Chem. Soc.* **2015**, *137*, 3886; c) D. Deng, Y. Zhang, J. Zhang, Z. Wang, L. Zhu, J. Fang, B. Xia, Z. Wang, K. Lu, W. Ma, Z. Wei, *Nat. Commun.* **2016**, *7*, 13740; d) J. Wan, X. Xu, G. Zhang, Y. Li, K. Feng, Q. Peng, *Energy Environ. Sci.* **2017**, *10*, 1739.
- [6] a) R. Wu, L. Yin, Y. Li, *Sci. China Mater.* **2016**, *59*, 371; b) S. D. Collins, N. A. Ran, M. C. Heiber, T.-Q. Nguyen, *Adv. Energy Mater.* **2017**, *7*, 1602242; c) L. Lu, T. Zheng, Q. Wu, A. M. Schneider, D. Zhao, L. Yu, *Chem. Rev.* **2015**, *115*, 12666; d) C. Liu, K. Wang, X. Gong, A. J. Heeger, *Chem. Soc. Rev.* **2015**, *45*, 4825; e) C. Cai, L. Huo, Y. Sun, *Adv. Mater.* **2017**, *29*, 1605437; f) T. Liu, X. Pan, X. Meng, Y. Liu, D. Wei, W. Ma, L. Huo, X. Sun, T. H. Lee, M. Huang, H. Choi, T. Kim, J. Y. Kim, W. C. H. Choy, Y. Sun, *Adv. Mater.* **2017**, *29*, 1602451.

- [7] a)W. Ma, J. R. Tumbleston, M. Wang, E. Gann, F. Huang, H. Ade, *Adv. Energy Mater.* **2013**, *3*, 864; b)M. Lenes, S. W. Shelton, A. B. Sieval, D. F. Kronholm, J. C. Hummelen, M. Blom, *Adv. Funct. Mater.* **2009**, *19*, 3002; c)R. B. Ross, C. M. Cardona, D. M. Guldi, S. G. Sankaranarayanan, M. O. Reese, N. Kopidakis, J. Peet, B. Walker, G. C. Bazan, E. Van Keuren, B. C. Holloway, M. Drees, *Nat. Mater.* **2009**, *8*, 208.
- [8] a)Y. Lin, X. Zhan, *Adv. Energy Mater.* **2015**, *5*, 1501063; b) C. B. Nielsen, S. Holliday, H.-Y. Chen, S. J. Cryer, I. McCulloch, *Acc. Chem. Res.* **2015**, *48*, 2803; c)W. Chen, Q. Zhang, *J. Mater. Chem. C* **2017**, *5*, 1275; d)W. Zhao, D. Qian, S. Zhan, S. Li, O. Inganäs, F. Gao, J. Hou, *Adv. Mater.* **2016**, *28*, 4734; e)S.-Q. Zhang, J.-H. Hou, *Acta Phys. –Chim. Sin.* **2017**, *33*, 2327.
- [9] a)Y. Yang, Z. Zhang, H. Bin, S. Chen, L. Gao, L. Xue, C. Yang, Y. Li, *J. Am. Chem. Soc.* **2016**, *138*, 15011; b)S. Dai, F. Zhao, Q. Zhang, T.-K. Lau, T. Li, K. Liu, Q. Ling, C. Wang, X. Lu, W. You, X. Zhan, *J. Am. Chem. Soc.* **2017**, *139*, 1336; c)S. Li, Y. Long, W. Zhao, S. Zhang, S. Mukherjee, H. Ade, J. Hou, *Adv. Mater.* **2016**, *28*, 9423; d)F. Zhao, S. Dai, Y. Wu, Q. Zhang, J. Wang, L. Jiang, Q. Ling, Z. Wei, W. Ma, W. You, C. Wang, X. Zhan, *Adv. Mater.* **2017**, *29*, 1700144; e)H. Bin, L. Gao, Z.-G. Zhang, Y. Yang, Y. Zhang, C. Zhang, S. Chen, L. Xue, C. Yang, M. Xiao, Y. Li, *Nat. Commun.* **2016**, *7*, 13651; f)D. Baran, R. S. Ashraf, D. A. Hanifi, M. Abdelsamie, N. Gasparini, J. A. Röhr, S. Holliday, A. Wadsworth, S. Lockett, M. Neophytou, *Nat. Mater.* **2016**, *16*, 4797; g)F. Liu, Z. Zhou, C. Zhang, T. Vergote, H. Fan, F. Liu, X. Zhu, *J. Am. Chem. Soc.* **2016**, *138*, 15523; h)D. Xie, T. Liu, W. Gao, C. Zheng, L. Huo, Z. Luo, K. Wu, W. Xiong, F. Liu, Y. Sun, C. Yang, *Solar. RRL* **2017**, *1*, 1700044; i)B. Kan, H. Feng, X. Wan, F. Liu, X. Ke, Y. Wang, Y. Wang, H. Zhang, C. Li, J. Hou, Y. Chen, *J. Am. Chem. Soc.* **2017**, *139*, 4929; j)D. Meng, D. Sun, C. Zhong, T. Liu, B. Fan, L. Huo, Y. Li, W. Jiang, H. Choi, T. Kim, J. Y. Kim, Y. Sun, Z. Wang, A. J. Heeger, *J. Am. Chem. Soc.* **2016**, *138*, 375; k)T. Liu, Y. Guo, Y. Yi, L. Huo, X. Xue, X. Sun, H. Fu, W. Xiong, D. Meng, Z. Wang, F. Liu, T. P. Russell, Y. Sun, *Adv. Mater.* **2016**, *28*, 10008; l)K. Zhang, X.-Y. Liu, B.-W. Xu, Y. Cui, M.-L. Sun, J.-H. Hou, *Chinese J. Polym. Sci.* **2017**, *35*, 219.
- [10] a)H. Shi, W. Fu, M. Shi, J. Ling, H. Chen, *J. Mater. Chem. A* **2014**, *3*, 1902; b)M. Saito, I. Osaka, Y. Suda, H. Yoshida, K. Takimiya, *Adv. Mater.* **2016**, *28*, 6921; c)G. Qiu, Z. Jiang, Z. Ni, H. Wang, H. Dong, J. Zhang, X. Zhang, Z. Shu, K. Lu, Y. Zhen, Z. Wei, W. Hu, *J. Mater. Chem. C* **2017**, *5*, 566.
- [11] a)A. Mishra, P. Bauerle, *Angew. Chem. Int. Ed.* **2012**, *51*, 2020; b)C. Zhan, X. Zhang, J. Yao, *RSC Adv.* **2015**, *5*, 93002; c)Y. Lin, X. Zhan, *Adv. Energy Mater.* **2015**, *5*, 1501063; d)M. E. Cinar, T. Ozturk, *Chem. Rev.* **2015**, *115*, 3036.
- [12] a)W. Li, L. Yang, J. R. Tumbleston, L. Yan, H. Ade, W. You, *Adv. Mater.* **2014**, *26*, 4456; b)X. Liu, Y. Sun, B. B. Hsu, A. Lorbach, L. Qi, A. J. Heeger, G. C. Bazan, *J. Am. Chem. Soc.* **2014**, *136*, 5697; c)M. T. Dang, L. Hirsch, G. Wantz, J. D. Wuest, *Chem. Rev.* **2013**, *113*, 3734.
- [13] a)I. McCulloch, M. Heeney, C. Bailey, K. Genevicius, I. MacDonald, M. Shkunov, D. Sparrowe, S. Tierney, R. Wagner, W. Zhang, M. L. Chabinc, R. J. Kline, M. D. McGehee, M. F. Toney, *Nat Mater* **2006**, *5*, 328; b)M. E. Cinar, T. Ozturk, *Chem Rev* **2015**, *115*, 3036; c)H.-H. Gao, Y. Sun, X. Wan, B. Kan, X. Ke, H. Zhang, C. Li, Y. Chen, *Sci. China Mater.* **2017**, *9*, 819.
- [14] a)Q. Zhang, Y. Wang, B. Kan, X. Wan, F. Liu, W. Ni, H. Feng, T. P. Russell, Y. Chen, *Chem. Commun.* **2015**, *51*, 15268; b)L. Zhang, F. Liu, Y. Diao, H. S. Marsh, N. S. Colella, A. Jayaraman, T. P. Russell, S. C. Mannsfeld, A. L. Briseno, *J. Am. Chem. Soc.* **2014**, *136*, 18120; c)D. Deng, S. Shen, J. Zhang, C. He, Z. Zhang, Y. Li, *Org. Electron.* **2012**, *13*, 2546.
- [15] a)I. McCulloch, M. Heeney, M. L. Chabinc, D. DeLongchamp, R. J. Kline, M. Cölle, W. Duffy, D. Fischer, D. Gundlach, B. Hamadani, R. Hamilton, L. Richter, A. Salleo, M. Shkunov, D. Sparrowe, S. Tierney, W. Zhang, *Adv. Mater.* **2009**, *21*, 1091; b)X. Guo, N. Zhou, S. J. Lou, J. Smith, D. B. Tice, J. W. Hennek, R. Ponce, Ortiz, J. T. Lopez, Navarrete, S. Li, J. Strzalka, L. X. Chen, R. P. H. Chang, A. Facchetti, T. J. Marks, *Nat. Photonics* **2013**, *7*, 825.
- [16] a)Y.-Y. Liu, C.-L. Song, W.-J. Zeng, K.-G. Zhou, Z.-F. Shi, C.-B. Ma, F. Yang, H.-L. Zhang, X. Gong, *J. Am. Chem. Soc.* **2010**, *132*, 16349; b)H. Xu, Y.-C. Zhou, X.-Y. Zhou, K. Liu, L. Y. Cao, Y. Ai, Z.-P. Fan, H.-L. Zhang, *Adv. Funct. Mater.* **2014**, *24*, 2907; c)J. Zaumseil, H. Sirringhaus, *Chem. Rev.* **2007**, *107*, 1296.
- [17] H. Yong, Y. Li, *Phys. Chem. Chem. Phys.* **2011**, *13*, 1970.
- [18] C. M. Proctor, M. Kuik, T.-Q. Nguyen, *Prog. Polym. Sci.* **2013**, *38*, 1941.
- [19] a)P. W. Blom, V. D. Mihailetschi, L. J. A. Koster, D. E. Markov, *Adv. Mater.* **2007**, *19*, 1551; b)J. L. Wu, F. C. Chen, Y. S. Hsiao, F. C. Chien, P. Chen, C. H. Kuo, M. H. Huang, C. S. Hsu, *ACS Nano* **2011**, *5*, 959.
- [20] F. Liu, Y. Gu, X. Shen, S. Ferdous, H. W. Wang, T. P. Russell, *Prog. Polym. Sci.* **2013**, *38*.
- [21] M. Zhang, X. Guo, W. Ma, H. Ade, J. Hou, *Adv. Mater.* **2014**, *26*, 5880.
- [22] (a)Y. Liu, X. Wan, F. Wang, J. Zhou, G. Long, J. Tian, Y. Chen, *Adv. Mater.* **2011**, *23*, 5387; b)Q. Zhang, B. Kan, F. Liu, G. Long, X. Wan, X. Chen, Y. Zuo, W. Ni, H. Zhang, M. Li, Z. Hu, F. Huang, Y. Cao, Z. Liang, M. Zhang, T. P. Russell, Y. Chen, *Nat. Photonics* **2015**, *9*, 35.